Diffusion of actin filaments within a thin layer between two walls

Guanglai Li and Jay X. Tang*
Physics Department, Brown University, Providence, Rhode Island 02912, USA
(Received 18 December 2002; published 23 June 2004)

Diffusion of the protein filaments *F*-actin confined in a thin layer between two walls is studied using the methods of single filament fluorescence imaging and particle tracking. The translational and rotational diffusion coefficients are measured for *F*-actin of lengths in the range of 1.5–5 μm. The length dependence of the measured diffusion coefficients is consistent with the predicted two-dimensional projection of the diffusion of a cylinder in an unbounded fluid. Fits based on the formulas for diffusion in the bulk fluid yield higher apparent viscosity values than that of the buffer solution by a factor of 2 for a layer thickness between 0.7 and 1.6 μm. We show that the measured results can be accounted for by correction based on the hydrodynamic theory of a long cylinder between confining walls.

DOI: 10.1103/PhysRevE.69.061921 PACS number(s): 87.15.Tt, 87.15.Vv

I. INTRODUCTION

The hydrodynamic theory [1–4] of a cylinder moving in a viscous fluid was verified on the macroscopic level by measuring the settling of individual metal rods [5]. Features such as the end effects and the anisotropy in drag coefficients along and perpendicular to the rod axis were observed. On the macromolecule level, sedimentation of DNA fragments yields coefficients that agree with the predictions of the hydrodynamic theory [6]. Another way to verify the theory on the molecular level is to measure the diffusion coefficients of rodlike molecules in a dilute solution [7]. The translational diffusion coefficient D is related to the drag coefficient ξ by the Einstein relation $D=k_BT/\xi$. These diffusion coefficients of macromolecules are typically measured by bulk methods such as dynamic light scattering and electric or flow birefringence decay [7,8]. Since all these bulk techniques involve a large ensemble of molecules, the behavior of individual molecules cannot be revealed. This limitation is particularly severe for systems of polydispersed sizes and filament lengths, such as self-assembled micelles and protein filaments. A growing number of examples in recent years demonstrate valuable information that can be acquired by single molecule techniques [9,10].

Macromolecules in cells constantly undergo Brownian motion. The hydrodynamics of these molecules is thus essential to biological processes. Many important macromolecules inside the cells are filamentous in their functional form, such as DNA, actin filaments (*F*-actin), and microtubules. *F*-actin, in particular, is the primary cytoskeletal component responsible for an elastic cell body, shape changes, and cellular migration. Recently, hydrodynamic theories of a cylinder in either an unbounded fluid or close to a wall [3,4,11] have been applied to determine the force on *F*-actin or microtubules generated by their respective molecular motors that balance the viscous drag force in *in vitro* motility assays [12–16]. However, due to the microscopic scale of cells, the motions of these protein filaments in confined geometries need to be carefully examined in comparison with hydrodynamic theories.

In this paper, we study the motions of *F*-actin confined in a thin layer between two glass walls. We use the established single-particle tracking technique [7,9,10] to measure the translational and rotational diffusion coefficients of *F*-actin. The movement of individual actin filaments is tracked, and their positions and orientations are measured to calculate diffusion coefficients. Our results show that diffusion coefficients of individual confined filaments are smaller than those in unbounded fluid by factors that can be estimated based on hydrodynamic theory.

II. EXPERIMENTS

F-actin was polymerized from the globular monomers *G*-actin by adding 50 mM KCl and 2 mM $MgCl_2$ into the protein solution initially containing 0.2 mM $CaCl_2$, 0.5 mM ATP, 0.5 mM DTT, and 2.0 mM Tris-HCl buffer, pH 7.95 at room temperature. A solution containing the same concentrations of all the ions listed is referred to as *F*-buffer, which was used to dilute *F*-actin. *F*-actin was labeled at a molar ratio of 1:1 with TRITC phalloidin [17] (Sigma, St. Louis, MO). Before making a sample for fluorescence microscopy, a stock solution of 0.4 mg/mL *F*-actin was diluted using *F*-buffer to 1 μg/mL. To reduce the effect of photobleaching, an antibleaching protocol was followed by adding 20 μg/mL catalase, 0.5 mg/mL glucose, 0.1 mg/mL glucose oxidase, and 0.25 vol% mercaptoethanol into the sample solution. Both glass slides and cover slips were incubated in 1 mg/mL BSA in *F*-buffer for at least 30 min before use.

A drop of 50 μL *F*-actin solution was added on a glass slide and then covered with a cover slip. Excess solution was removed with a filter paper quickly after the cover slip was pressed against the slide to yield a thin sample. This sample was then sealed with vacuum grease. The sample was used to record the motions of *F*-actin, and calculate translational and rotational diffusion constants. A Nikon Eclipse E800 epifluorescence microscope with a 60× oil immersion objective

*Author to whom correspondence should be addressed. Email address: Jay_Tang@Brown.edu

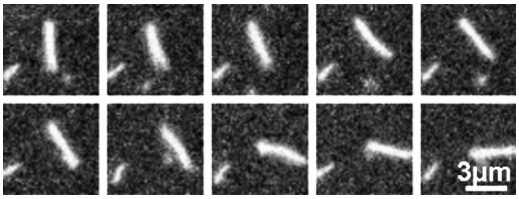

FIG. 1. Sequential fluorescence images of a 3.2 μm long actin filament taken at 0.1 s interval, showing its translational and rotational motions. A shorter filament partially stuck to the surface at the bottom-left corner serves as a good position marker.

lens was used to image the labeled *F*-actin. Motions of *F*-actin were recorded at a rate of 10 frames per second by a Cool-Snap CCD camera (Roper Scientific, NJ), controlled by *MetaMorph* software (Universal Imaging Co., IN).

The following method was used to measure the thickness of the gap between a cover slip and a glass slide. Cover slips and glass slides were coated with a film of Ag approximately 30 nm thick by thermal evaporation. The Ag film was then scratched off, showing parallel lines with approximately 200 μm spacing. Samples for optical microscopy were made following the same procedure as described in the paragraph above using these partially coated glass slides and cover slips. The lines on the cover slip were placed perpendicular to those on the glass slide and therefore square windows formed for microscopy observation. The focus on the Ag film at the edges of the windows of either the cover slip or the glass slide was carefully adjusted under the phase contrast mode of the microscope. The translation read directly from the *z* knob of the microscope was calibrated by measuring an optical fiber of known diameter submersed under the same solution. The measured separations varied between 0.7 and 1.6 μm, with an average value of 1.2 μm.

The viscosity of *F*-buffer, including chemicals specified in the antiphotobleaching protocol, was measured by an Advanced Rheometer (TA Instruments) using a cuvette cell of 9 mL sample volume. The measured viscosity was 0.82×10^{-3} Pa s at 23°C, with an estimated 10% error. This value agrees with the known value for water, which is 0.89×10^{-3} Pa s at 23°C.

III. RESULTS

Actin filaments were observed to stay within the focal plane despite the translational and rotational Brownian motions. This is due to the fact that the sample thickness is comparable with the depth of field of the 60× objective lens, and therefore all images are actually two-dimensional projections of the moving filaments. Figure 1 shows 10 sequential frames of a 3.2-μm-long *F*-actin taken at 0.1 s time intervals. Although a tilt of the filament away from the plane of view is generally expected, both the center-of-mass position and the orientation of the filament projected on the focal plane can be measured in each frame. The translational diffusion coefficient D_t of a single filament was calculated using $\langle \Delta r^2 \rangle = 4D_t \Delta t$, where $\langle \Delta r^2 \rangle$ is the mean-square displacement in the center-of-mass position over the time interval Δt. The rotational diffusion coefficient D_r was calculated from

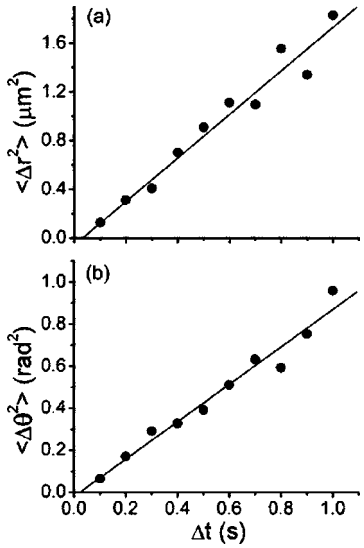

FIG. 2. Representative plots for obtaining translational (a) and rotational diffusion constants (b), respectively.

$\langle \Delta \theta^2 \rangle = 2D_r \Delta t$, where $\langle \Delta \theta^2 \rangle$ is the mean-square rotation of *F*-actin over Δt. More than 100 positions and angles were measured for each selected filament. The mean-square displacements $\langle \Delta r^2 \rangle$ and $\langle \Delta \theta^2 \rangle$ were obtained using internal averaging [18]; that is, all position pairs with time interval Δt were included. Examples of calculations of translational and rotational diffusion constants are shown in Figs. 2(a) and 2(b), respectively. The diffusion coefficient was obtained by a linear fit to the first few Δt values. Due to the limited number of measured positions and angles, using a larger Δt value beyond the range shown in the plots does not reduce further the error in calculation [18]. In this paper, only the first four time intervals of 0.1 s, 0.2 s, 0.3 s, and 0.4 s are used for the fitting. Applying the linear fits as shown in Fig. 2 greatly reduces the error in the calculated diffusion coefficients caused by errors in measurements of positions and angles. Note that the translational and rotational diffusion constants are calculated from motions projected onto the focal plane, thus corresponding to a two-dimensional diffusion for translation and a one-dimensional diffusion for rotation, respectively.

Both translational and rotational diffusion coefficients were determined for *F*-actin with various lengths up to 5 μm [Figs. 3(a) and 3(b)]. Since these filaments are much shorter than the persistence length of *F*-actin [19,20], they are treated as rigid rods in comparison with the hydrodynamic theory of diffusion. Optical spread due to diffraction causes an apparent increase to the length as well as the diameter of the filament. The increase to the filament length was assumed to be equal to the increase in diameter, which was determined to be 0.4 μm for an immobilized *F*-actin.

Secondly, an actin filament is generally tilted in the gap while it undergoes Brownian motion. Both effects give rise to additional blurring at the ends of the filament. The projection of a tilted filament would yield a shorter length, which compensates for the blurring of the ends due to the tilt. The error caused by diffusion is better assessed and is estimated as the root-mean-square displacement due to Brownian mo-

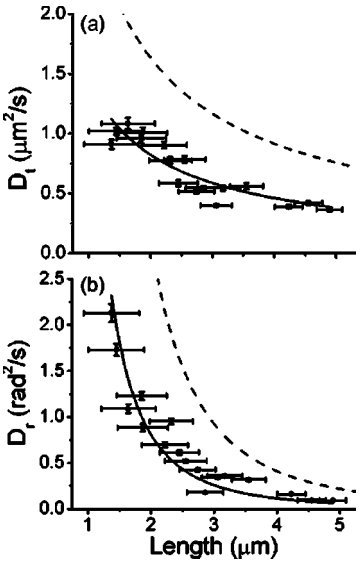

FIG. 3. (a) The orientation-averaged translational diffusion coefficient plotted as a function of the *F*-actin length. The solid line is a fit to Eq. (1), which yields an apparent viscosity $\eta=1.71\times10^{-3}$ Pa s. (b) Rotational diffusion coefficient plotted as a function of *F*-actin length. The solid line is a fit to Eq. (2), which yields an apparent viscosity $\eta=2.62\times10^{-3}$ Pa s. The dashed lines represent calculated bulk values, using 0.89×10^{-3} Pa s as the viscosity for water at 23°C.

tion $\sqrt{2D_{//}\Delta t}$, where $D_{//}$ is the translational diffusion coefficient along the filament. The estimated errors depend on the filament length, and are indicated by the size of the error bars in Figs. 3 and 5.

The measured diffusion constants are compared with the corresponding diffusion constants in bulk fluid. When a rodlike macromolecule is in an unbounded fluid, its translational diffusion coefficients along and perpendicular to the rod axis are given by

$$D_{//}=\frac{k_BT[\ln(L/d)+\gamma_{//}]}{2\pi\eta L},$$

$$D_{\perp}=\frac{k_BT[\ln(L/d)+\gamma_{\perp}]}{4\pi\eta L}.$$

The two-dimensional translational diffusion coefficient is

$$D_t=\frac{k_BT[3\ln(L/d)+2\gamma_{//}+\gamma_{\perp}]}{8\pi\eta L}. \quad (1)$$

The rotational diffusion coefficient is

$$D_r=\frac{3k_BT[\ln(L/d)+\gamma_r]}{\pi\eta L^3}, \quad (2)$$

where k_B is the Boltzmann constant, T is the temperature, L and d are the length and diameter of the rodlike molecule, η is the viscosity of the surrounding liquid, and $\gamma_{//}$, $\gamma_{\perp}$, and γ_r are the end-correction coefficients [4]. For $L/d=\infty$, Broersma [4] gave the values $\gamma_{//}=-0.114$, $\gamma_{\perp}=0.886$, and $\gamma_r=-0.447$.

The calculated translational and rotational diffusion coefficients in unbounded fluid from Eqs. (1) and (2) are plotted as dashed lines in Figs. 3(a) and 3(b), respectively. These bulk values are bigger than those measured for *F*-actin confined between the two walls. The solid lines correspond to a fit of Eqs. (1) and (2) to the experimental results for translational and rotational diffusion coefficients, respectively, taking η as a fit parameter. The value of η that yields the best fit is hereafter referred to as an apparent viscosity. Neither D_t nor D_r is sensitive to the filament diameter, which we set to be 8 nm for *F*-actin. Varying the effective hydrodynamic radius by a factor of 2 results in a less than 15% change of viscosity in the fit.

The apparent viscosities are $\eta=1.71\times10^{-3}$ Pa s for translational diffusion and $\eta=2.62\times10^{-3}$ Pa s for rotational diffusion. A major source of error in fitting comes from uncertainty in the measured *F*-actin length, as discussed above. As an alternative treatment, we consider both an upper limit and a lower limit of filament length within the error for the fitting, which give a lower limit and an upper limit of apparent viscosity, respectively. Fitting the data to the expression of the translational diffusion coefficient yields $\eta=(1.47-1.98)\times10^{-3}$ Pa s, and to that of the rotational diffusion coefficient yields $\eta=(1.41-4.99)\times10^{-3}$ Pa s. Fitting of several other samples resulted in apparent viscosity values that are comparable to the values shown here. The fits clearly show the length dependence of the diffusion coefficients. The rotational diffusion coefficient is much more sensitive to length than the translational diffusion coefficient. Due to the big error in length measurement, there is a big error in apparent viscosity obtained by fitting the rotational diffusion coefficients. Therefore, the apparent viscosity fit for the translational diffusion is more reliable.

The apparent viscosity based on the translational diffusion of *F*-actin in the confined thin layer is about twice that predicted in the bulk water. Nevertheless, our results show that if we simply assume a higher apparent viscosity, diffusion of the confined *F*-actin scales satisfactorily with the filament length as predicted by the theory for a bulk dilute solution. In the discussion section below we show that the functional dependence for the confined filament is the same as bulk hydrodynamic theory following adjustment of a single fit parameter.

IV. DISCUSSION

From the Einstein relationship $D=k_BT/\xi$, the diffusion coefficient D is inversely proportional to the drag coefficient ξ. Thus the smaller diffusion constants of *F*-actin confined between two walls correspond to larger drag coefficients compared to those in unbounded fluid.

A cylinder feels a larger drag when it is closer to a wall. For an infinitely long cylinder parallel to a wall, the drag coefficient per unit length for motion parallel to the cylinder axis is [13]

$$c_{//}=2\pi\eta/\cosh^{-1}(h/r), \quad (3)$$

where h is the distance from the cylinder axis to the wall and r is the radius of the cylinder. For motions perpendicular to

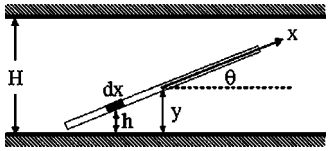

FIG. 4. State of a thin rod between two walls. θ is the angle between the filament axis and the wall, and y is the distance of the rod center from the bottom wall. H is the thickness of the gap between the walls. The x axis is along the filament axis originated at the center of the rod.

the cylinder axis and parallel to the wall, the drag coefficient per unit length is twice that of $c_{//}$, i.e., $c_{\perp}=2c_{//}$.

However, in our case, *F*-actin is not always parallel to the walls. Figure 4 shows the side view of a typical state of a rod defined by (y,θ), where y is the center-of-mass position and θ is its tilt angle from the surface. It is reasonable to assume that the rod has an equal opportunity to explore each state. For each state, the drag coefficient is denoted as $\xi(y,\theta)$.

The overall diffusion coefficient is calculated from the diffusion constant D_i for each state (y_i,θ_i). For the translational diffusion constant, $\langle \Delta r_i^2 \rangle = 4D_{ti}\Delta t$. Since each state has an equal probability, the overall translational diffusion coefficient of the filament can be expressed as follows:

$$\langle \Delta r^2 \rangle = \frac{1}{N}\sum_{i=1}^{N} \langle \Delta r_i^2 \rangle = 4\frac{1}{N}\sum_{i=1}^{N} D_{ti}\Delta t = 4D_t\Delta t.$$

Therefore the overall translational diffusion constant is an average over the diffusion constants of all possible states,

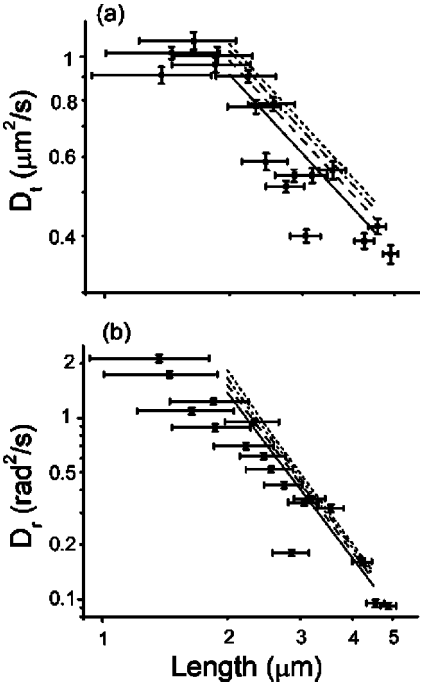

FIG. 5. Comparison of the calculated and measured translational (a) and rotational (b) diffusion coefficients. Both axes are scaled logarithmically. The four lines in each figure are calculated using Eqs. (4) and (5) with the gap thickness H of, from bottom to top, 0.7, 1.0, 1.3, and 1.6 μm, respectively.

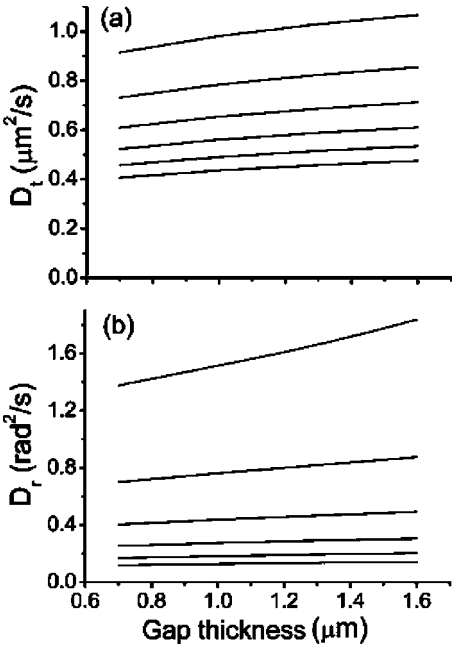

FIG. 6. Translational (a) and rotational (b) diffusion coefficients calculated from Eqs. (4) and (5) for *F*-actin of several filament lengths as functions of gap thickness. Curves in each figure are calculated for *F*-actin of 2.0, 2.5, 3.0, 3.5, 4.0, and 4.5 μm long from top to bottom.

$D_t=\langle D_{ti}\rangle$. The same is true for the rotational diffusion constant.

To calculate the diffusion constant, we need to know the drag coefficient at each state. Two assumptions are made. (i) The drag coefficients per unit length $c_{//}$ and $c_{\perp}$ of a section of cylinder dx (see Fig. 4) with distance h from the bottom wall are expressed by Eq. (3). This assumption is less prone to error for longer cylinders in narrower gaps. (ii) The total drag on the section dx is a sum of the drags by the two walls. Therefore, for each state the total drag coefficient of the whole cylinder along the axis is

$$\xi_{//}(y,\theta) = \int_{-L/2}^{L/2} \left(\frac{2\pi\eta}{\cosh^{-1}[(y + x\ \sin\ \theta)/r]} + \frac{2\pi\eta}{\cosh^{-1}[(H - y - x\ \sin\ \theta)/r]} \right) dx.$$

The drag coefficient perpendicular to the cylindrical axis is twice that of the value expressed above, i.e., $\xi_{\perp}(y,\theta) = 2\xi_{//}(y,\theta)$. The two-dimensional translational diffusion coefficient in this state is

$$D_t(y,\theta) = (D_{//}\cos^2\theta + D_{\perp} + D_{\perp}\sin^2\theta)/2 = \left(\frac{k_BT}{\xi_{//}(y,\theta)}\cos^2\theta + \frac{k_BT}{\xi_{\perp}(y,\theta)}(1+\sin^2\theta) \right) \Big/ 2.$$

Averaged over all states, the overall translational diffusion constant is

$$D_t = \frac{\int_0^{H/2} dy \int_{-\sin^{-1}(2y/L)}^{\sin^{-1}(2y/L)} D_t(y,\theta) d\theta}{\int_0^{H/2} dy \int_{-\sin^{-1}(2y/L)}^{\sin^{-1}(2y/L)} d\theta}. \quad (4)$$

When the rod rotates with an angular velocity ω around an axis through the center of the rod and perpendicular to the walls for the state (y,θ), the torque on the rod is

$$\Gamma(y,\theta) = \int_{-L/2}^{L/2} c_\perp \omega\, x^2 \cos^2\theta\, dx.$$

Accordingly, the rotational drag coefficient is

$$\xi_r(y,\theta) = \Gamma(y,\theta)/\omega = \int_{-L/2}^{L/2} \left(\frac{4\pi\eta\, x^2 \cos^2\theta}{\cosh^{-1}[(y + x\sin\theta)/r]} + \frac{4\pi\eta\, x^2 \cos^2\theta}{\cosh^{-1}[(H - y - x\sin\theta)/r]} \right) dx$$

and the rotational diffusion coefficient is

$$D_r(y,\theta) = k_B T/\xi_r(y,\theta).$$

Finally, the overall rotational diffusion coefficient is

$$D_r = \frac{\int_0^{H/2} dy \int_{-\sin^{-1}(2y/L)}^{\sin^{-1}(2y/L)} D_r(y,\theta) d\theta}{\int_0^{H/2} dy \int_{-\sin^{-1}(2y/L)}^{\sin^{-1}(2y/L)} d\theta}. \quad (5)$$

Numerical calculations of Eqs. (4) and (5) are shown in Figs. 5(a) and 5(b), plotted logarithmically in comparison with the experimental data as shown earlier in Fig. 3. Diffusion constants of *F*-actin 2–5 μm in lengths confined in gaps of thickness 0.7, 1.0, 1.3, and 1.6 μm are calculated. The gap thicknesses selected correspond to the gap thicknesses in our experiments. The calculated values of diffusion coefficients are slightly larger than the experimental ones, and the calculated diffusion coefficients for the narrower gap fit the experimental values better than calculations for the wider gaps, which implies a smaller gap thickness in the experiments. The calculated diffusion coefficients show clearly a length dependence of L^{-1} for the translational diffusion coefficient and L^{-3} for the rotational diffusion coefficient.

The dependence of the calculated diffusion coefficient on gap thickness is intuitive. The narrower the gap, the smaller the diffusion constant. It is important to note, however, that within the range of the gap thickness in our experiments, the diffusion constants vary only slightly with the gap thickness [Figs. 6(a) and 6(b)]. Therefore, the diffusion coefficients measured in different samples or at different sample locations with the gap thicknesses in the range of 0.7–1.6 μm can practically be shown in the same figure. With this approximation, all the measured diffusion coefficients exhibit a common functional dependence with the filament length as if they were measured for a fixed gap thickness.

V. CONCLUDING REMARKS

We have combined the methods of fluorescence microscopy and single filament tracking to study the diffusion of *F*-actin within a thin layer confined between two walls. The measured translational and rotational diffusion coefficients are smaller than those of two-dimensional diffusion in an unbounded fluid. However, the hydrodynamic theory of diffusion for cylinders in a boundary-free fluid can be applied to fit the measured diffusion coefficients, using a higher apparent viscosity. The origin of the lower diffusion coefficients in confined layers has been discussed. By applying the drag coefficient of an infinitely long cylinder next to a confining wall, the diffusion coefficients are calculated, which fit the measured results.

ACKNOWLEDGMENTS

This work was supported by NSF-DMR9988389 and NIH R01 HL67286. We thank Qi Wen for helping with the numerical calculations, and Professor A. Tripathi for the viscosity measurement.

[1] S. Broersma, J. Chem. Phys. **32**, 1626 (1960).
[2] S. Broersma, J. Chem. Phys. **32**, 1632 (1960).
[3] M. M. Tirado and J. d. l. Torre, J. Chem. Phys. **71**, 2581 (1979).
[4] S. Broersma, J. Chem. Phys. **74**, 6989 (1981).
[5] J. F. Feiss and J. Coull, Chem. Eng. Prog. **48**, 133 (1952).
[6] R. T. Kovacic and K. E. V. Holde, Biochemistry **16**, 1490 (1977).
[7] M. M. Tirado, C. L. Martínez, and J. G. d. l. Torre, J. Chem. Phys. **81**, 2047 (1984).
[8] W. Eimer and R. Pecora, J. Chem. Phys. **94**, 2324 (1991).
[9] M. Goulian and S. M. Simon, Biophys. J. **79**, 2188 (2000).
[10] M. P. Sheetz *et al.*, Nature (London) **340**, 284 (1989).
[11] D. J. Jeffrey and Y. Onishi, Q. J. Mech. Appl. Math. **34**, 129 (1981).
[12] A. J. Hunt and J. Howard, Proc. Natl. Acad. Sci. U.S.A. **90**, 11 653 (1993).
[13] A. J. Hunt, F. Gittes, and J. Howard, Biophys. J. **67**, 766 (1994).
[14] O. Pänke *et al.*, Biophys. J. **81**, 1220 (2001).
[15] D. Riveline *et al.*, Eur. Biophys. J. **27**, 403 (1998).
[16] R. Yasuda *et al.*, Cell **93**, 1117 (1998).
[17] J. Käs *et al.*, Biophys. J. **70**, 609 (1996).
[18] M. J. Saxton, Biophys. J. **72**, 1744 (1997).
[19] F. Gittes *et al.*, J. Cell Biol. **120**, 923 (1993).
[20] L. Le Goff *et al.*, Phys. Rev. Lett. **89**, 258101 (2002).